Star-shaped furoate-PCL: An effective compound for the development of graphite nanoplatelets-based films

(Article begins on next page)

08 September 2024

Star-Shaped Furoate-PCL: an Effective Compound for the Development of Graphite Nanoplatelets-based Films

Giacomo Damonte[1], Francesco Cantamessa[2], Alberto Fina[2], Orietta Monticelli[1*]

[1]Dipartimento di Chimica e Chimica Industriale, Università degli studi di Genova, Via Dodecaneso 31, 16146 Genoa, Italy;

[2]Dipartimento di Scienza Applicata e Tecnologia, Politecnico di Torino-sede di Alessandria, Viale Teresa Michel, 5, 15121 Alessandria, Italy

Abstract. The aim of this study was to improve the dispersibility of graphite nanoplatelets (GNP) in films based on poly(ε-caprolactone) (PCL). To this end, a star-shaped PCL with furoate-like end groups (PCL-Fur), potentially capable of interacting/reacting with the surface of the graphene layers through Diels-Alder reactions, was synthesized by enzymatic catalysis. PCL-Fur was applied for film development by blending it with a commercial high molecular weight PCL (PCL-L) and GNP. The reactivity of GNP with respect to furoate groups was demonstrated by studying the thermal behavior of the GNP/methyl 2-furoate system, while the dispersibility of graphite in the solution containing PCL-Fur was studied by UV-Vis measurements. GNP proved to be well dispersed and adhered to the polymer matrix in the PCL-L/PCL-Fur/GNP composite films prepared by casting, in contrast to the films based on the neat PCL-L. This fine GNP dispersion resulted in films characterized by high electrical conductivity.

1. Introduction

The dispersion of graphene-related materials (GRM) in polymers represents an important and widely studied aspect for the production of high performance systems [1]. Indeed, although the exploitation of such fillers/nanofillers, such as graphite nanoplatelets (GNP), can improve the mechanical and thermal properties and, most importantly, increase the electrical and thermal conductivity of the polymer, these performances are closely related to the GRM dispersion in the matrix. In the case of biopolymers, the improvement of their properties is an even more important issue that is being studied in order to make these systems competitive with those from fossil sources and not biodegradable. Among the various biopolymers of academic and industrial interest, poly(ε-caprolactone) (PCL) was considered in this work for its wide range of applications [2]. Indeed, its biocompatibility properties make it a polymer that can be used in the biomedical field [3], while its elongation and biodegradation allow it to be applied alone or in combination with other polymers in the packaging field [4]. Concerning the formation of polymer/GRM systems, the dispersion of GRM can be promoted by modifying the structure of the nanofiller [5] or that of the polymer [6]. In the first case, the surface of graphite can generally be oxidized, making the resulting graphite oxide or graphene oxide (GO) much more compatible with polar polymers [7]. In addition, GO can be further functionalized to improve its compatibility with the polymer matrix [8-10]. For example, the above approach was described for polypropylene (PP)-based systems in which GO reacted with 4,4-diphenylmethane diisocyanate (MDI) and then stearic acid to form functionalized sheets, which exhibited strong interfacial adhesion with PP [8] and promoted the orientation of PP crystallites [10].

In the case of PCL, there are several examples dealing with the combination of this polymer with GO, especially in the context of the formation of nanofibers made by electrospinning [11]. Despite the easy dispersibility of GO, oxidation is naturally associated with a reduction of electrical and

thermal conductivity, which can be restored by the use of strong chemical reducing agents [12] and/or high temperatures [13]. Therefore, modifying the polymer structure to increase the affinity of the polymer with the nanofiller surface seems to be a promising route. Indeed, star-shaped or linear PCLs ending with pyrene groups, able to interact with the graphite surface through π-stacking-like interactions have been recently synthesized [14,15]. The resulting PCL/GNP systems, characterized by a fine nanofiller dispersion, exhibited high thermal and electrical conductivity. In this work, we extended the application of PCL, by moving from a polymer with functionalities which promote the dispersion of GNP through specific interactions to a PCL with groups capable not only of interacting with graphene layers but also of reacting with them. Thus, a star-shaped PCL ending with furan-type functional groups (PCL-Fur) which can act as a diene in Diels-Alder (DA) reactions with edges [16,17] and defects, normally present on the surface of graphite nanoplates, was synthesized [16-18] (Figure 1). The material was specifically designed for the preparation of dense films. To this end, PCL-Fur, characterized by a star-shaped architecture and low molecular weight to maximize end functionalities, prepared from a hydroxyl-terminated polymer, the synthesis of which was previously reported by the authors [15,19], was mixed with a high molecular weight linear commercial polymer suitable for film development.

Indeed, as described in literature, blends consisting of branched polymers with arms of the same type as the main polymer are fully miscible [20]. To obtain a high efficiency and sustainable functionalization, the furoate polymer was synthesized by enzymatic catalysis. The films, consisting of a linear high molecular weight commercial PCL (PCL-L), PCL-Fur and GNP, were prepared by solvent casting and characterized to evaluate their thermal, and electrical conductivity properties (Figure 1). In addition, the properties of the developed systems were compared with those of films made of PCL-L, PCL-Fur and the composite with GNP dispersed in PCL-L.
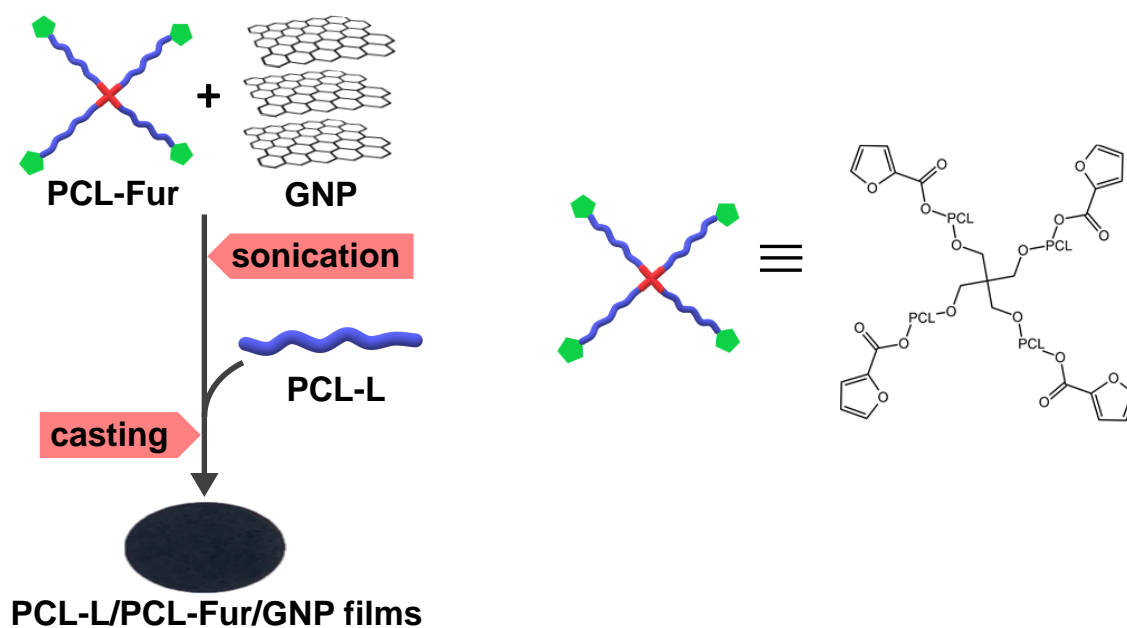
Figure 1. Scheme of PCL-L/PCL-Fur/GNP film preparation procedure.

2. Materials and methods

2.1. Materials

ε-caprolactone, methanol, tin octanoate (Sn(Oct)$_2$), dichloromethane (DCM), methyl-2-furoate, acetonitrile, anhydrous toluene, calcium hydride, deuterated chloroform (CDCl$_3$), acetone were purchased by Sigma-Aldrich. High molecular weight (M_w = 50000 g/mol) PCL CAPA 6500$^®$ (hereafter referred to as PCL-L) was obtained from Perstorp (Sweden). Immobilized Candida Antarctica Lipase B (CALB) Novozyme 435$^®$ was purchased by Novozymes$^®$. Graphite nanoplatelets (GNP), with BET surface area of 196 m^2/g, were supplied by Avanzare Innovacion Tecnologica (Navarrete, Spain). ε-caprolactone was distilled over CaH$_2$ under reduced pressure. All the other reagents were used directly as received without purification.

2.2. Synthesis of furoate-PCL (PCL-Fur)

The furoate PCL (hereafter referred to as PCL-Fur) was synthesized starting from a star-shaped hydroxyl-terminated PCL (hereafter referred to as PCL-OH), prepared by ring opening polymerization (ROP) of ε-caprolactone in bulk, using pentaerythritol as initiator and Sn(Oct)$_2$ as catalyst, according to a procedure reported in the literature [21]. Specifically, ε-caprolactone was added to a 50-mL two-neck round bottom flask purged with argon gas, followed by the proper amount of initiator to achieve the desired molecular weight of 2000 g/mol per arm. The system was then gently heated to 80 °C with stirring to dissolve the initiator in the monomer and produce a homogeneous solution. When the mixture was clear, the temperature was increased to 120 °C with stirring and Sn(Oct)$_2$ was added as a 100 mg/ml solution in anhydrous toluene to maintain the ratio [ε-CL]/[Sn(Oct)$_2$] = 5000. After 24 h, the warm crude polymer was dissolved in an equal amount of DCM. The purified product was obtained as a fine powder by slowly dropping the solution into a large volume of ice-cold methanol with vigorous stirring (50 mL/g PCL). This was filtered through a Büchner funnel, washed several times with small volumes of fresh methanol, and dried in vacuum at 30 °C for 72 h.

IR signals of PCL-OH: 2945 cm^{-1} (asymmetric -**CH$_2$**- stretching); 2870 cm^{-1} (symmetric -**CH$_2$**- stretching); 1725 cm^{-1} (symmetric >**C=O** stretching); 1297 cm^{-1} (-**C-O**- and -**C-C**- stretching); 1242 cm^{-1} (asymmetric -**C-O-C**- stretching); 1179 cm^{-1} (symmetric -**C-O-C**- stretching).

^{1}H-NMR chemical shifts of PCL-OH: 4.09 ppm (-**CH$_2$**- pentaerythritol, s); 4.05 ppm (-**CH$_2$**-, t); 3.63 ppm (-**CH$_2$**-OH PCL chain terminal, t); 2.31 ppm (-**CH$_2$**-, t); 1.65 (-**CH$_2$**-, m); 1.38 (ppm -**CH$_2$**-, m).

PCL-Fur was synthesized by enzimatic esterification of the synthesized PCL-OH with CALB, as previously reported [22] (Figure 2). To a two-necked round bottomed flask equipped with a stir bar and flowed with argon, 1 g PCL-OH (1 eq.), 78.8 µL methyl 2-furoate (6 eq.), 78.8 mg CALB

(equal quantity as methyl 2-furoate) and 3 mL anhydrous toluene were added. The system was then stirred at 60 °C for 72 h. At the end of the reaction, the solution was filtered to remove the enzyme on the acrylic resin beads. The polymer was then precipitated from cold methanol (50 ml/g), filtered through a Büchner funnel, and washed several times with small portions of ice-cold methanol. The polymer was dried in a vacuum oven at 30 °C for 72 hours.
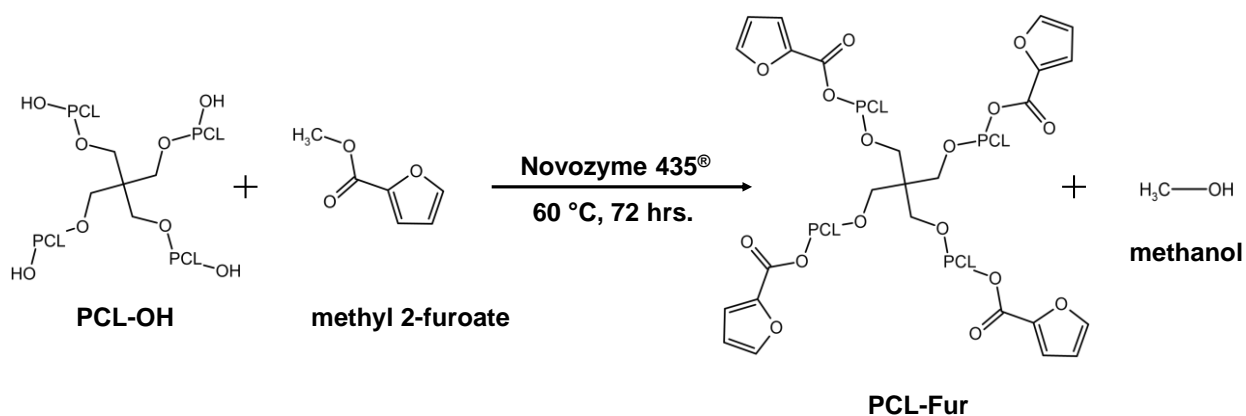

Figure 2. Reaction scheme of the enzymatic furoylation reaction of PCL-OH.

2.3. Film preparation procedure

Polymer films were prepared from DCM solution by solvent casting. Specifically, 10 ml of DCM containing 200 mg of the neat PCL-L or the mixture PCL-L/PCL-Fur with a ratio 80/20, was poured into a Petri dish with an inner diameter of 54 mm. To prepare the GNP-containing films, the appropriate amount of GNP (1 or 2 wt.% based on the total polymer content) was dispersed in the solvent together with PCL-Fur by sonication in a sonication bath at 40 kHz for two h. After the sonication phase, the high molecular weight PCL-L was added with stirring to obtain a homogeneous dispersion of GNP, maintaining the PCL-L/PCL-Fur ratio at 80/20. The films were then prepared by slowly evaporating the solvent for 24 h at 30 °C in an oven. To remove the remaining solvent, the films were then released from the Petri dishes and placed in vacuum oven for additional 48 h at 30 °C. The films were defined by indicating in the code GNP concentration (as an

example: PCL-L/PCL-Fur/G1 indicates a film prepared with a GNP concentration of 1 wt.% and with a ratio PCL-L/PCL-Fur of 80/20).

2.4. Characterization

FT-IR analysis was performed on polymer films using a Bruker "Vertex 70®" in ATR mode in the range 400-4000 cm^{-1}. ^{1}H-NMR spectroscopy was performed with a JEOL ECZ400R/S3 at a frequency of 400 MHz using 10 mm NMR tubes and CDCl$_3$ as solvent at r.t. DSC analysis of the films was performed using a Mettler Toledo "DSC1 STARe System®" in the temperature range of -100 to 150 °C at a heating rate of 10 °C/min and a nitrogen flow of 20 ml/min. The degree of crystallinity (Xc) of PCL in the films was then calculated using Equation (1)

$$X_c = \frac{\Delta H_m}{\Delta H_m^0} \cdot 100 \qquad (1)$$

where ΔH_m = fusion enthalpy (measured in the second heating scan) and ΔH_m^0 = fusion enthalpy of a 100% crystalline PCL, a value found in the literature (139 J/g) [23].

To study the Diels-Alder (DA) reaction between GNP and the furoate-type functionalities, 35 mg of GNP was sonicated in 4 ml of methyl 2-furoate for one h. The mixture was then allowed to react at 30 °C for 72 hours, the same time and temperature as for the film preparation. The modified GNP was then obtained by centrifugation (three times at 6000 g for 5 min, washing the material each time with fresh acetone) and dried at room temperature. The retro DA was evaluated by DSC analysis in a single heating scan from 0 to 150 °C at a heating rate of 10 °C/min and a nitrogen flow of 20 ml/min.

TGA was performed using a Mettler Toledo "TGA/DSC1 STARe System®" from 30 °C to 800 °C with a heating rate of 10 °C/min under a nitrogen atmosphere of 80 mL/min. UV-Vis spectra were recorded with a Shimadzu® UV 1800 UV-Vis spectrometer in the 200-400 nm range using quartz cells in acetonitrile solution.

Conductivity measurements were performed at room temperature on rectangular films (dimensions: length 30 mm, width 5 mm, thickness approximately 0.08 mm) connected with flat copper clamps (10 mm wide to ensure full contact over the entire sample width), at a distance of 20 mm and connected to a current generator set to 150 V cc. The current flow through the sample was measured using a picoammeter (Keithley Instruments, Solon, OH, USA) and then the material conductivity was calculated by applying Ohm's laws.

3. Results and discussion

3.1. PCL-Fur characterization

To confirm the functionalization of the star-shaped PCL-OH, its FT-IR spectrum was compared with that of PCL-Fur (Figure 3a). For both the synthesized polymers, all signals typical of PCL [24] can be detected at 2945 cm^{-1} (asymmetric -**CH$_2$**- stretching); 2870 cm^{-1} (symmetric -**CH$_2$**- stretching); 1725 cm^{-1} (symmetric >**C=O** stretching); 1297 cm^{-1} (-**C-O**- and -**C-C**- stretching); 1242 cm^{-1} (asymmetric -**C-O-C**- stretching); 1179 cm^{-1} (symmetric -**C-O-C**- stretching). Additional signals were observed in the spectrum of PCL-Fur at 1580 cm^{-1} (**C=C** stretching furan) and 886 cm^{-1}, 768 cm^{-1}, 616 cm^{-1} (furan ring vibrational motions), which can be attributed to 2-furoate unit [25]. This finding preliminarily corroborated the functionalization of the polymer after the esterification reaction.
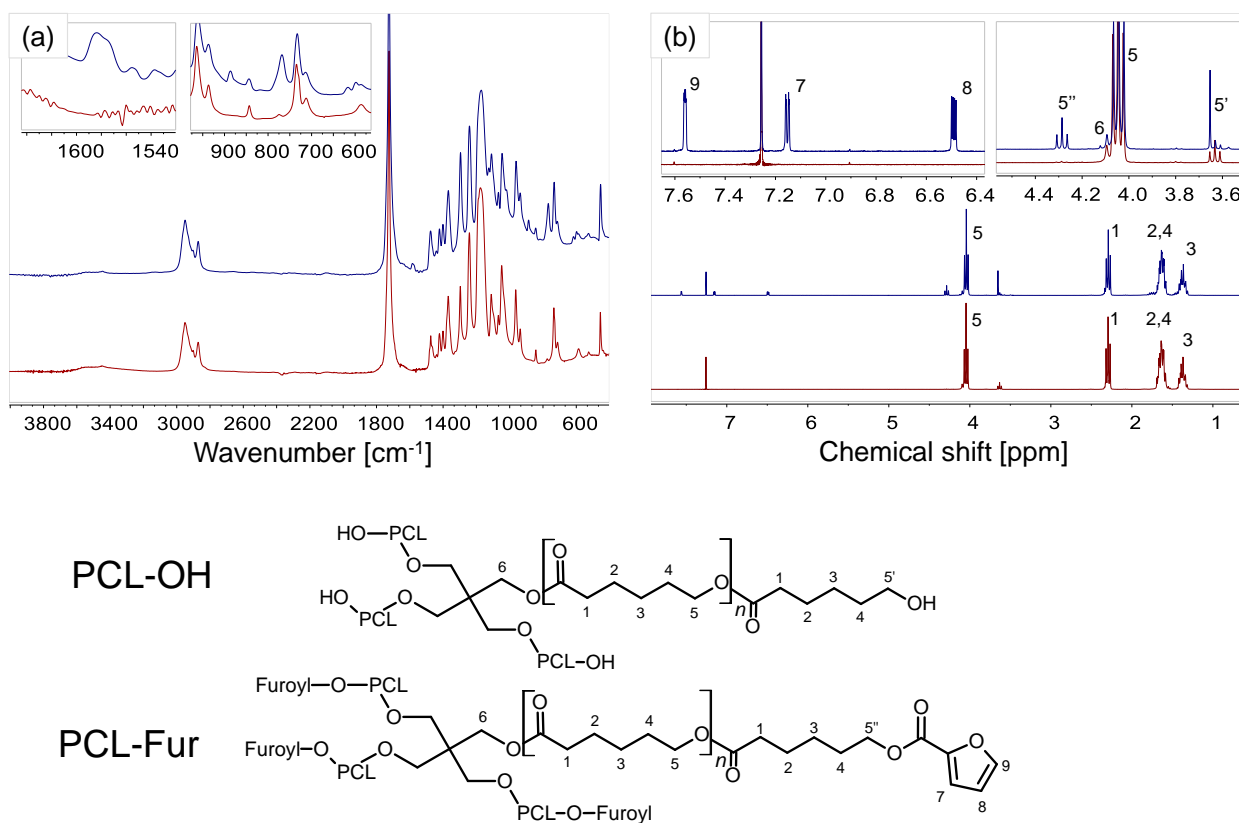
Figure 3. FT-IR (a) and ^{1}H-NMR (b) spectra of: PCL-OH (red) and PCL-Fur (blue). The polymer structures are indicated below with proton numbering for the sake of clarity.

^{1}H-NMR spectra of PCL-OH and PCL-Fur are reported in Figure 3b. For both polymers, typical signals of PCL can be observed [26] at 4.09 ppm (6, -CH_2- pentaerythritol, s); 4.05 ppm (5, -CH_2-, t); 2.31 ppm (1, -CH_2-, t); 1.65 pp (2 and 4, -CH_2-, m); 1.38 ppm (3, -CH_2-, m). In the spectrum of PCL-OH, the presence of a signal at 3.65 ppm (5', -CH_2-OH PCL chain terminal, t) indicates the presence of hydroxyl groups. In contrast, in PCL-Fur spectrum, the occurrence of the esterification was proven by the presence of the furan proton signals at 7.58 ppm (9, furan -CH-, dd); 7.17 ppm (7, furan -CH-, dd); 6.50 ppm (8, furan -CH-, dd); and by the formation of a new signal at 4.30 ppm (5", -CH_2-O-furoyl PCL chain terminal, t), demonstrating the esterification of hydroxyl end groups of PCL-OH [15,27].

From the evaluation of M_{nNMR}, calculated from the ratio between the areas of the signals of terminals and chain protons ($A_{5'}/A_1$ for PCL-OH and $A_{5''+5'}/A_1$ for PCL-Fur), a decrease in the molecular weight of the star-shaped PCL was observed after the enzymatic esterification reaction. Indeed, the M_{nNMR} value went from 2000 g/mol per arm for the PCL-OH to about 1400 g/mol in PCL-Fur. The above decrease in molecular weight was probably caused by a depolymerization process due to the effect of CALB on the PCL ester bonds. Nevertheless, the polymer obtained is suitable for the intended purpose due to the high degree of functionalization (ca. 80%).

To verify the effects of functionalization on the thermal properties of the star-shaped polymer, both PCL-OH and PCL-Fur were characterized by DSC and TGA measurements (Figure S1 and Table S1). In particular, PCL-OH showed values of crystallization temperature (T_c), melting temperature (T_m) and degree of crystallinity (χ_c) in perfect agreement with those reported in the literature for four-arm PCL with similar molecular weight [15,28]. It was found that esterification does not significantly change the thermal properties of the polymer, since only a slight change in the crystallization and melting temperature (T_c from 28 °C for PCL-OH to 25 °C for PCL-Fur, T_m from 49 °C for PCL-OH to 46 °C for PCL-Fur) was observed. In the case of PCL-Fur, the double peak in the heating curve can be ascribed to the crystal lamellae thickness distribution produced during crystallization [14], which is possibly affected by the presence of furoate end groups.

As for the TGA analysis, the values of the onset of degradation temperature (T_{onset}) and the maximum rate of degradation temperature (T_{max}) of PCL-OH, which are consistent with those previously reported for polymers with similar features [15], are related to an unzipping-type degradation mechanism, as a consequence of the hydroxyl end groups of the star-shaped polymer. Interestingly, the esterified polymer exhibited higher T_{onset} and T_{max} with respect to PCL-OH. This phenomenon can be explained by the fact that the esterification of the hydroxyl end groups in PCL-Fur suppresses the unzipping mechanism and thus favors β-elimination, a mechanism typical of

high molecular weight PCL [15,29]. Indeed, this finding provides further support for the esterification of PCL-OH hydroxyl end groups.

3.4. Study of interactions/reactions of furoate functionalities with GNP and GNP dispersibility

To verify the interactions/reactions of the furoate group with the graphene layers, the thermal behavior of the mixture of GNP and methyl 2-furoate was investigated treating it at the same temperature and time of the film preparation process, as reported in the Experimental Section. It is worth underling that the analysis of the DSC trace can provide information about the reaction between the above compound and GNP, since the direct Diels-Alder (DA) reaction, which can occur between the furoate functionalities, acting as diene, and the graphene layers defects, acting as dienophile, is exothermic and reversible [30]. Therefore, once the bond is formed, it may be possible to reverse the reaction (retro DA) and then break the formed bond by simple heating. Methyl-2-furoate was chosen as a probe molecule to maximise the extent of functionalization and thus the signal obtained, taking into account of the relatively low concentration of the furoate as terminal groups in the star shaped PCL. In addition, since PCL melts at about 60 °C, its endothermic melting peak may mask the endothermic peak associated with DA transitions. Indeed, in order to focus on the above reaction, a heating scan was performed in the range 0 °C - 150 °C. From the thermogram in Figure 4a, it can be seen that the curve of neat GNP is completely flat in the studied temperature range, clearly indicating the absence of a thermal transition. On the other hand, the methyl 2-furoate/GNP sample showed a broad peak at about 80 °C, which can be attributed to the process of retro DA, as described in the literature for other furan-based systems [31]. This observation brings evidence the ability of furan derivatives to serve as a source of reversible networks in graphene-containing materials. Based on these findings, the same furoate-GNP interaction is expected between the star-shaped PCL end groups and the GNP surface, which can be exploited to promote dispersion of graphite in the polymer matrix.
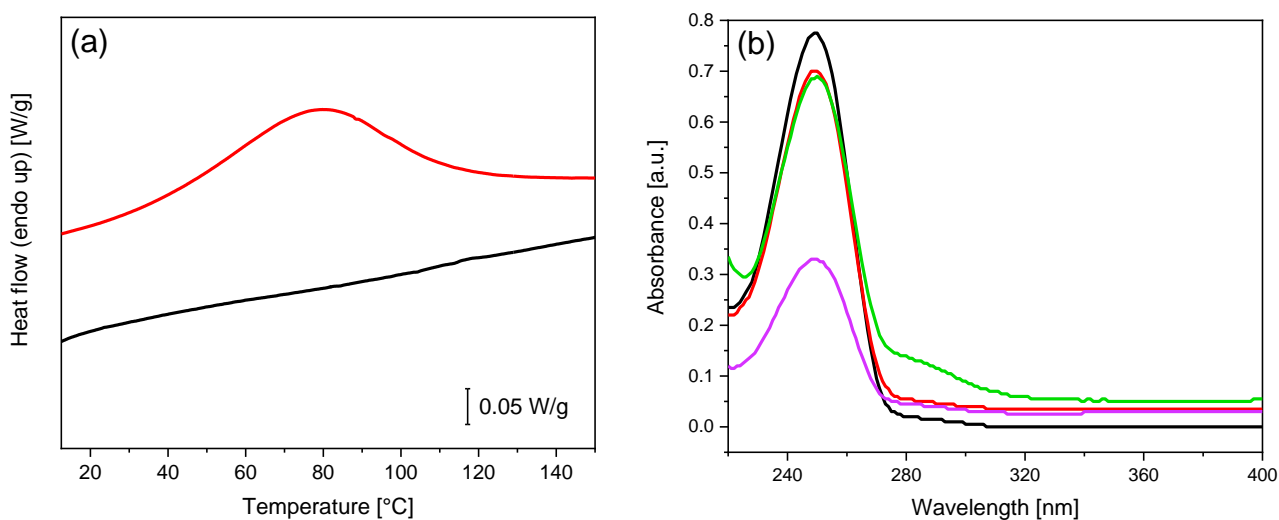
Figure 4. (a) DSC trace of methyl 2-furoate/GNP mixture (red curve) and pristine GNP (black curve). (b) Comparison between the UV-Vis spectra of the dispersions of PCL-Fur (black curve) with different concentrations of graphite in acetonitrile (1 mg red, 2 mg green, 5 mg violet curve).

To investigate the effect of PCL-Fur on the dispersibility of GNP, different solutions containing a fixed amount of this polymer in acetonitrile were sonicated together with different quantities of GNP (1, 2 and 5 mg) and allowed to sediment for one week. In Figure 4b, the UV-Vis spectra of the leftover surnatant of dispersions remaining after the sedimentation time are reported. A peak at 250 nm was observed in all the analyzed samples, which can be attributed to the absorption of the furoate group [32]. It is relevant to underline that the intensity of the above peak decreased with increasing GNP content in the system. This finding indicates a direct decrease in the PCL-Fur content in the solution and, especially for the system with the highest GNP concentration (5 mg), the ability of GNP to interact with the polymer, causing its adsorption and consequently its concentration decrease in the solution. Moreover, in the sample containing 2 mg of GNP, a shoulder was visible at about 290 nm, which, as previously reported [14,33], can be related to the absorption caused by the dispersed graphite.

13

3.5. Characterization of blend and composite films.

The prepared composite films were preliminarily characterized from a morphological point of view. Figure 5 compares the photo and Figure S2 the optical microscopy image of PCL-L/PCL-Fur/G2 film containing 2 wt.% of GNP with a film prepared by adding the same amount of nanofiller to the neat PCL (PCL-L/G2).
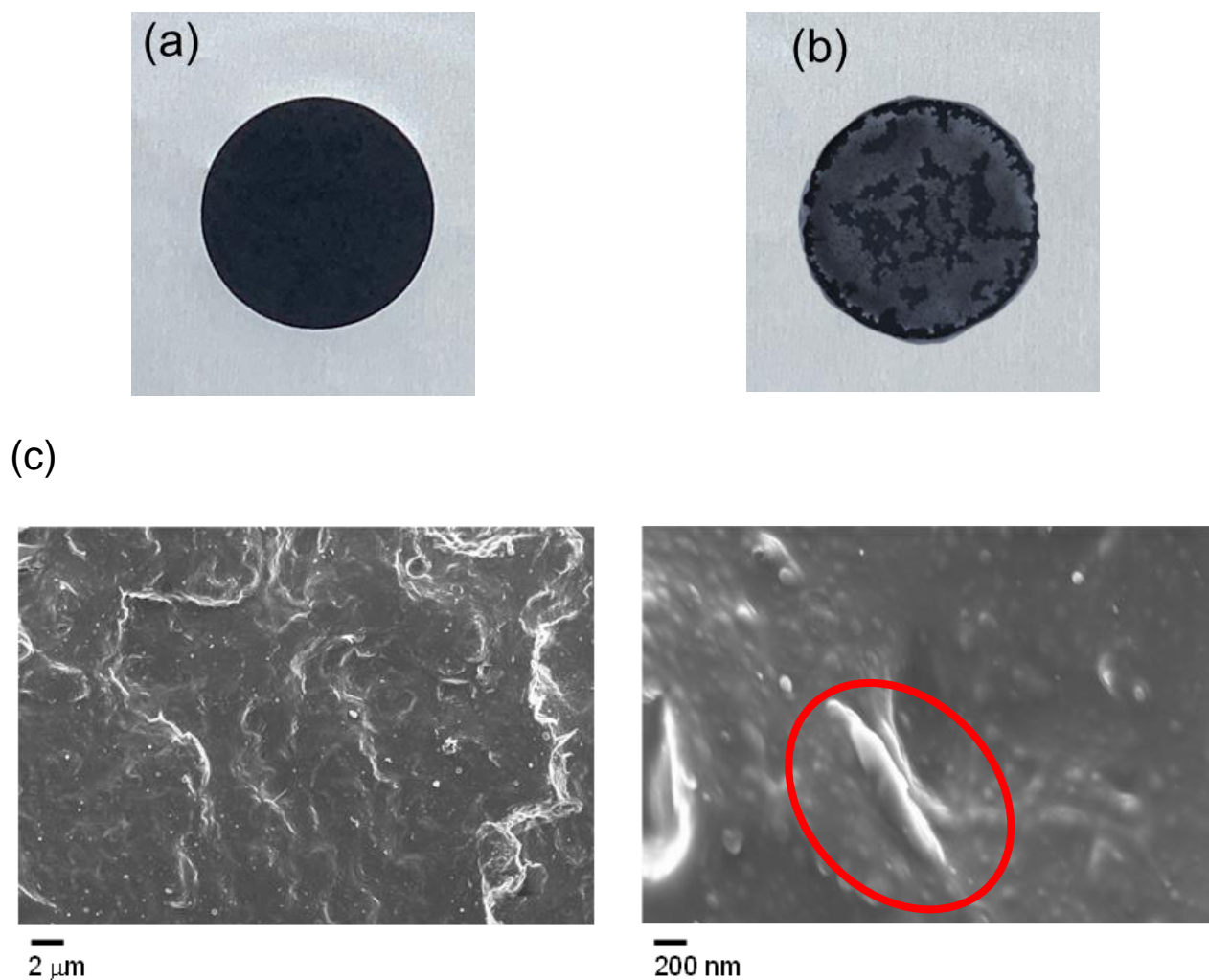

Figure 5. Photos of: (a) PCL-L/PCL-Fur/G2 and (b) PCL-L /G2. (c) FE-SEM micrographs of PCL-L/PCL-Fur/G2 at different magnifications.

It is evident that PCL/G2 film is extremely inhomogeneous with visible aggregates. In contrast, PCL/PCL-Fur/G2 film, prepared under the same conditions as the previous one, is characterized by a homogeneous graphite dispersion, which is evident by the absence of visible GNP agglomerates. FE-SEM measurements, carried out only on the sample which showed visible homogeneity, allowed to study in detail the dispersion of GNP in the cross-section of the polymer films. The micrographs shown in Figure 5c refer to PCL-L/PCL-Fur/G2, the morphology of the sample with 2 wt.% graphite, PCL-L/PCL-Fur/G1 being very similar. The analysis of these micrographs reveals that the GNP was well distributed in the cross-section of the film, and higher magnification in particular shows that they also adhered well to the polymer (see GNP highlighted within the red circle). This result can be attributed to the specific interactions/reactions that can occur between GNP and the furoate groups of PCL-Fur, which is rich in functionalities thanks to its star-shaped architecture. The above system indeed proved to be homogeneously dispersed in the PCL matrix, since it is characterized by arms of the same chemical nature and its interactions with the graphite ensure a similarly good dispersion.
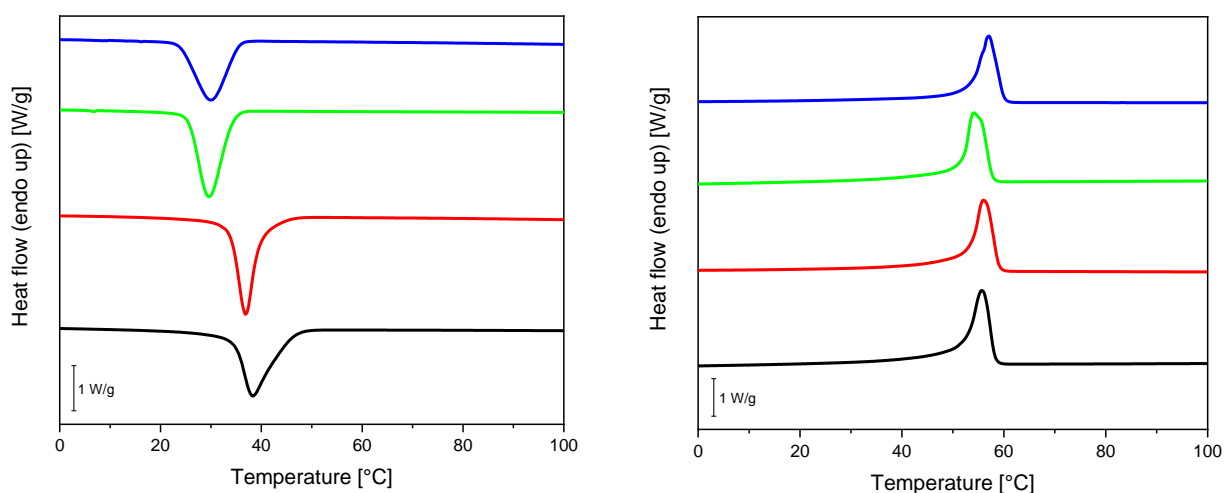

Figure 6. DSC thermograms, second heating (left) and cooling (right) of: PCL-L (blue curve), PCL-L/PCL-Fur (green curve), PCL-L/PCL-Fur/G1 (red curve) and PCL-L/PCL-Fur/G2 (black curve).

Table 1. Thermal properties of the prepared films.

Sample code	ΔH_c [J/g]	T_c [°C]	ΔH_m [J/g]	T_m [°C]	X_c [%]	T_{onset} [°C]	T_{max} [°C]
PCL-L	-56	30	69	57	50	388	426
PCL-L/PCL-Fur	-78	30	80	54	57	382	428
PCL-L/PCL-Fur/G1	-65	37	78	56	57	389	428
PCL-L/PCL-Fur/G2	-82	38	84	55	62	388	428

The subscript m and c indicate the values measured during melting and crystallization, respectively. X_c is the degree of crystallinity calculated by assuming the ideal enthalpies of fusion as 139 J/g. T_{onset} and T_{max} indicate the onset of the degradation temperature at a weight loss of 5 % and the maximum rate of degradation temperature, respectively.

The thermal properties of the neat films based on PCL-L and the blend PCL-L/PCL-Fur were compared with those of the composite films containing 1 wt% and 2 wt% GNP (PCL-L/PCL-Fur/G1 and PCL-L/PCL-Fur/G2). The DSC traces are shown in Figure 6, while the results are summarized in Table 1. The crystallization temperature (T_c), melting temperature (T_m) and crystallinity (X_c) of the PCL-L-based film are in agreement with the values reported in the literature [34,35]. The film obtained by mixing the two polymers (PCL-L/PCL-Fur) exhibited a slightly higher crystallinity than PCL-L, with X_c increasing from 50 % for PCL-L to 57 % for PCL-L/PCL-Fur, a phenomenon probably due to the presence of the furoate polymer in the mixture, which is characterized a higher crystallinity because of its lower molecular weight. It worth underlining that only one melting temperature appeared in the thermogram of the blend system, indicating the complete miscibility between PCL-L and PCL-Fur. An increase in crystallization temperature for the GNP-containing samples was found, with T_c increasing from 30 °C for the neat samples to 37 °C and 38 °C in the presence of 1 or 2% wt. GNP, respectively. As described in the literature [14,15], this result can be attributed to the nucleating effect of GNP. Regarding the thermal

decomposition, all the prepared films showed similar T_{onset} and T_{max}. Indeed, the weight loss decomposition step occurred in the range between 400-450 °C, indicating a decomposition that follows a β-elimination mechanism as described in the literature [36].

The effect of GNP on the electrical properties of the prepared films was evaluated by comparing the conductivity (σ) of the neat PCL-L and PCL-L/PCL-Fur films with those of the GNP-based films (Figure 7). As can be seen from the histogram, both PCL-L and the PCL-L/PCL-Fur blend were found to be insulating materials with σ in the range of 10^{-12} S·m^{-1}. However, the presence of GNP resulted in a significant increase in the measured current flow and thus in the conductivity of the films. In particular, the addition of 1 wt.% GNP in PCL-L/PCL-Fur/G1 led to an increase in conductivity to a value of $1.1 \cdot 10^{-10}$ S·m^{-1}, while PCL-L/PCL-Fur/G2, containing 2 wt.% of GNP reached a value of $4.3 \cdot 10^{-3}$ S·m^{-1}, namely seven orders of magnitude higher than PCL-L/PCL-Fur/G1 and nine higher than PCL-L and PCL-L/PCL-Fur. It is worth underling that the conductivity found for PCL-L/PCL-Fur/G2 is among the highest values reported for PCL/GRM systems, characterized by the same filler content [14,37]. This result can be attributed to the formation of an efficient percolative network within the polymer matrix [38]. The conversion point from insulator to conductor is observed here between 1 and 2% wt., confirming the fine GNP dispersion, which may be ascribed to the interactions/reactions between the star-shaped furoate polymer and GNP.
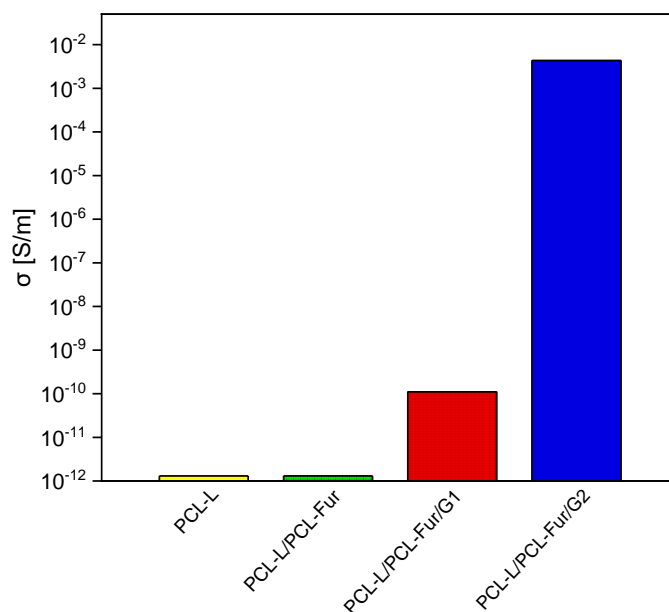
Figure 7. Conductivity of neat PCL-L and PCL-L/PCL-Fur films and the films based on GNP.

4. Conclusions

In this work, a strategy was developed to render films based on PCL electrically conductive. The approach is based not only on the addition of GNP to the polymer matrix, but also on the blending a high molecular weight PCL (PCL-L) with a star-shaped PCL (PCL-Fur) synthesized *ad-hoc* by an environmentally friendly enzymatic functionalization process. The arms of the star-shaped polymer, being of the same nature as the matrix, ensured a good miscibility in the system, while the furoate-like end groups, capable of reacting via Diels-Alder reaction with the surface of the graphene layers, promoted GNP dispersion. Consequently, PCL-L/PCL-Fur/G2 composite film based on 2 wt.% GNP exhibited a surface conductivity among the highest found in the literature for this type of system. The "green" nature of the polymer matrix, as well as the final properties of the material and its simple preparation procedure, make the developed system attractive for application in various fields. In the biomedical field, for example, one can imagine the development of scaffolds

containing drugs that can be released by electrical stimulation, while in the field of packaging, ductile conductive films can be used for electronic components.

References

[1]   S. Perumal, R. Atchudan, I.W. Cheong, Recent studies on dispersion of graphene–polymer composites, Polymers 13 (2021) 2375. https://doi.org/10.3390/polym13142375.

[2]   M. Labeta, W. Thielemans, Synthesis of polycaprolactone: a review, Chem. Soc. Rev. 38 (2009) 3484–3504. https://doi.org/10.1039/b820162p

[3]   E. Malikmammadov, T.E. Tanir, A. Kiziltay, V. Hasirci, N. Hasirci, PCL and PCL-based materials in biomedical applications, J. Biomater. Sci. Polym. Ed. 29 (2018) 863–893. https://doi.org/10.1080/09205063.2017.1394711.

[4]   J.S. Lyu, J.-S. Lee, J. Han, Development of a biodegradable polycaprolactone film incorporated with an antimicrobial agent via an extrusion process, Sci. Rep. 9 (2019) 20236. https://doi.org/10.1038/s41598-019-56757-5.

[5]   D. Razzaghi, M. Rezaei, A. Babaie, The effect of incorporating graphene and polycaprolactone-grafted graphene oxide nanosheets on thermal and physico-mechanical properties, microstructure and biocompatibility of electrospun polyurethane nanocomposite mats, Compos. Part B Eng. 224 (2021) 109210. https://doi.org/10.1016/j.compositesb.2021.109210.

[6]   A. Fina, S. Colonna, L. Maddalena, M. Tortello, O. Monticelli, Facile and low environmental impact approach to prepare thermally conductive nanocomposites based on polylactide and graphite nanoplatelets, ACS Sustain. Chem. Eng. 6 (2018) 14340–14347. https://doi.org/10.1021/acssuschemeng.8b03013.

[7]   M. Sabzevari, D.E. Cree, L.D. Wilson, Graphene oxide-chitosan composite material for

treatment of a model dye effluent, ACS Omega 3 (2018) 13045–13054. https://doi.org/10.1021/acsomega.8b01871.

[8]   F. Qiu, Y. Hao, X. Li, B. Wang, M. Wang, Functionalized graphene sheets filled isotactic polypropylene nanocomposites, Compos. Part B Eng. 71 (2015) 175–183. https://doi.org/10.1016/j.compositesb.2014.11.027.

[9]   L. Gan, F. Qiu, Y.-B. Hao, K. Zhang, Z.-Y. Zhou, J.-B. Zeng, M. Wang, Shear-induced orientation of functional graphene oxide sheets in isotactic polypropylene, J. Mater. Sci. 51 (2016) 5185–5195. https://doi.org/10.1007/s10853-016-9820-z.

[10]   S. Pu, Y.-B. Hao, X.-X. Dai, P.-P. Zhang, J.-B. Zeng, M. Wang, Morphological, rheological, crystalline and mechanical properties of ethylene-vinyl acetate copolymer/linear low-density polyethylene/amphiphilic graphene oxide nanocomposites, Polym. Test. 63 (2017) 289–297. https://doi.org/10.1016/j.polymertesting.2017.08.028.

[11]   J. Song, H. Gao, G. Zhu, X. Cao, X. Shi, Y. Wang, The preparation and characterization of polycaprolactone/graphene oxide biocomposite nanofiber scaffolds and their application for directing cell behaviors, Carbon 95 (2015) 1039–1050. https://doi.org/10.1016/j.carbon.2015.09.011.

[12]   S. Pei, H.M. Cheng, The reduction of graphene oxide, Carbon 50 (2012) 3210–3228. https://doi.org/10.1016/j.carbon.2011.11.010.

[13]   M.M. Bernal, M. Tortello, S. Colonna, G. Saracco, A. Fina, Thermally and electrically conductive nanopapers from reduced graphene oxide: effect of nanoflakes thermal annealing on the film structure and properties, Nanomaterials 7 (2017) 2–8. https://doi.org/10.3390/nano7120428.

[14]   G. Damonte, A. Vallin, A. Fina, O. Monticelli, On the development of an effective method to produce conductive PCL film, Nanomaterials 11 (2021) 1385. https://doi.org/10.3390/nano11061385.

[15] G. Damonte, A. Vallin, D. Battegazzore, A. Fina, O. Monticelli, Synthesis and characterization of a novel star polycaprolactone to be applied in the development of graphite nanoplates-based nanopapers, React. Funct. Polym. 167 (2021) 105019. https://doi.org/10.1016/j.reactfunctpolym.2021.105019.

[16] Y. Cao, S. Osuna, Y. Liang, R.C. Haddon, K.N. Houk, Diels-alder reactions of graphene: computational predictions of products and sites of reaction, J. Am. Chem. Soc. 135 (2013) 17643–17649. https://doi.org/10.1021/ja410225u.

[17] P.A. Denis, Organic chemistry of graphene: the diels-alder reaction, Chem. - A Eur. J. 19 (2013) 15719–15725. https://doi.org/10.1002/chem.201302622.

[18] C.-R. Oh, S.-H. Lee, J.-H. Park, D.-S. Lee, Thermally self-healing graphene-nanoplate/polyurethane nanocomposites via diels–alder reaction through a one-shot process, Nanomaterials 9 (2019) 434. https://doi.org/10.3390/nano9030434.

[19] E.R. Leone, L.S. Ferraraccio, G. Damonte, P. Lova, P. Bertoncello, O. Monticelli, On the development of electrochemical sensors coated with polycaprolactone, Electrochem. Commun. 129 (2021) 107089. https://doi.org/10.1016/j.elecom.2021.107089.

[20] O. Monticelli, D. Oliva, S. Russo, C. Clausnitzer, P. Pötschke, B. Voit, On blends of polyamide 6 and a hyperbranched aramid, Macromol. Mater. Eng. 288 (2003) 318–325. https://doi.org/10.1002/mame.200390033.

[21] A.M. Bhayo, R. Abdul-Karim, S.G. Musharraf, M.I. Malik, Synthesis and characterization of 4-arm star-shaped amphiphilic block copolymers consisting of poly(ethylene oxide) and poly(ε-caprolactone), RSC Adv. 8 (2018) 28569–28580. https://doi.org/10.1039/c8ra05000g.

[22] W. Farhat, A. Biundo, A. Stamm, E. Malmström, P. Syrén, Lactone monomers obtained by enzyme catalysis and their use in reversible thermoresponsive networks, J. Appl. Polym. Sci. 137 (2020) 48949. https://doi.org/10.1002/app.48949.

[23] N. Gokalp, C. Ulker, Y.A. Guvenilir, Synthesis of polycaprolactone via ring opening

polymerization catalyzed by candida antarctica lipase b immobilized onto an amorphous silica support, J. Polym. Mater. 33 (2016) 87–100.

[24] M. Azizi, M. Azimzadeh, M. Afzali, M. Alafzadeh, S.H. Mirhosseini, Characterization and optimization of using calendula officinalis extract in the fabrication of polycaprolactone/gelatin electrospun nanofibers for wound dressing applications, J. Adv. Mater. Process. 6 (2018) 34–46.

[25] A.H.J. Cross, S.G.E. Stevens, T.H.E. Watts, Some characteristic infra-red absorption frequencies of furan compounds. I, J. Appl. Chem. 7 (2007) 562–565. https://doi.org/10.1002/jctb.5010071008.

[26] M. Sobczak, Ring-opening polymerization of cyclic esters in the presence of choline/SnOct$_2$ catalytic system, Polym. Bull. 68 (2012) 2219–2228. https://doi.org/10.1007/s00289-011-0676-8.

[27] T. Defize, R. Riva, J.-M. Raquez, P. Dubois, C. Jérôme, M. Alexandre, Thermoreversibly crosslinked poly(ε-caprolactone) as recyclable shape-memory polymer network, Macromol. Rapid Commun. 32 (2011) 1264–1269. https://doi.org/10.1002/marc.201100250.

[28] J.-L. Wang, C.-M. Dong, Physical properties, crystallization kinetics, and spherulitic growth of well-defined poly(ε-caprolactone)s with different arms, Polymer 47 (2006) 3218–3228. https://doi.org/10.1016/j.polymer.2006.02.047.

[29] G. Damonte, L. Maddalena, A. Fina, D. Cavallo, A.J. Müller, M.R. Caputo, A. Mariani, O. Monticelli, On novel hydrogels based on poly(2-hydroxyethyl acrylate) and polycaprolactone with improved mechanical properties prepared by frontal polymerization, Eur. Polym. J. 171 (2022) 111226. https://doi.org/10.1016/j.eurpolymj.2022.111226.

[30] K. Ramesh, D.S.B. Anugrah, A.K. Mishra, B.-H. Ahn, Y.-S. Gal, K.T. Lim, Green and sono synthetic approach for direct-functionalization of reduced graphene oxide with poly(styrene-alt-maleic anhydride) by diels alder "click" reaction, Appl. Surf. Sci. 504 (2020) 144482.

https://doi.org/10.1016/j.apsusc.2019.144482.

[31] C. Cai, Y. Zhang, M. Li, Y. Chen, R. Zhang, X. Wang, Q. Wu, T. Chen, P. Sun, Multiple-responsive shape memory polyacrylonitrile/graphene nanocomposites with rapid self-healing and recycling properties, RSC Adv. 8 (2018) 1225-1231. https://doi.org/10.1039/c7ra11484b.

[32] D.G. Manly, E.D. Amstutz, Ultraviolet spectra of 2-substituted furans and 5-substituted methyl furoates, J. Org. Chem. 22 (1957). https://doi.org/10.1021/jo01354a601.

[33] Y. Xu, J. Geng, X. Zheng, K.D. Dearn, X. Hu, Friction-induced transformation from graphite dispersed in esterified bio-oil to graphene, Tribol. Lett. 63 (2016). https://doi.org/10.1007/s11249-016-0708-5.

[34] Q. Ma, K. Shi, T. Su, Z. Wang, Biodegradation of polycaprolactone (pcl) with different molecular weights by candida antarctica lipase, J. Polym. Environ. 28 (2020) 2947-2955. https://doi.org/10.1007/s10924-020-01826-4.

[35] G. Damonte, B. Barsanti, A. Pellis, G.M. Guebitz, O. Monticelli, On the effective application of star-shaped polycaprolactones with different end functionalities to improve the properties of polylactic acid blend films, Eur. Polym. J. 176 (2022) 111402. https://doi.org/10.1016/j.eurpolymj.2022.111402.

[36] M. Unger, C. Vogel, H.W. Siesler, Molecular weight dependence of the thermal degradation of poly(ε-caprolactone): a thermogravimetric differential thermal fourier transform infrared spectroscopy study, Appl. Spectrosc. 64 (2010) 805–809. https://doi.org/10.1366/000370210791666309.

[37] E. Correa, M.E. Moncada, O.D. Gutiérrez, C.A. Vargas, V.H. Zapata, Characterization of polycaprolactone/rgo nanocomposite scaffolds obtained by electrospinning, Mater. Sci. Eng. C. 103 (2019) 109773. https://doi.org/10.1016/j.msec.2019.109773.

[38] Y.-D. Shi, J. Li, Y.-J. Tan, Y.-F. Chen, M. Wang, Percolation behavior of electromagnetic interference shielding in polymer/multi-walled carbon nanotube nanocomposites, Compos.

Sci. Technol. 170 (2019) 70–76. https://doi.org/10.1016/j.compscitech.2018.11.033.